

NiMo Nanoparticles Electrodeposited by Pulsed Current and Their Catalytic Properties for Hydrogen Production

Savidra Lucatero, Gabriel Tamayo, Diego Crespo, Ernesto Mariño and Marcelo Videá *

Department of Chemistry, Tecnológico de Monterrey, Campus Monterrey
Ave. E. Garza Sada 2501, 64849 Monterrey, N. L., México

Received: September 14, 2012, Accepted: February 18, 2013, Available online: July 08, 2013

Abstract: The electrocatalytic activity of NiMo nanoparticles (NPs) fabricated by means of current pulses from a binary electrolyte was characterized using cyclic voltammetry. The pulse current density, j_{pulse} , was varied in the range of 7 to 430 mA/cm², whereas the pulse time, t_{pulse} , was kept constant at two seconds. Mean NP size, D_{mean} , ranged within 27 and 38 nm at j_{pulse} values between 15 and 140 mA/cm²; with D_{mean} increasing as j_{pulse} was higher. NP dispersion (i. e., number of objects per unit area of substrate) was lower when j_{pulse} values were also low (15 and 35 mA/cm²), which showed consistency with a promoted nuclei formation and prolonged NP growth at higher j_{pulse} values. An improved catalytic performance for hydrogen evolution was determined upon increasing j_{pulse} in the range of 7 to 70 mA/cm² and remaining practically unvaried at higher j_{pulse} values. The electro-synthesis of two distinct catalytic materials was indicated by electrochemical characterization of deposits; the material with greatest catalytic activity also showed high instability, causing a dramatic decay (~80%) in the activity after two consecutive cycles of operation. Ni and Mo content in electrodeposits were both sensitive to variations in j_{pulse} .

Keywords: hydrogen, evolution, nanoparticles, electrodeposition, NiMo alloy

1. INTRODUCTION

The production and utilization of clean hydrogen fuel is a mean to diminish negative environmental effects caused by popular consumption of petroleum derivatives [1-3]. Hydrogen can be produced electrochemically from water and making use of a catalyst to facilitate electron transfer, such as platinum; a main drawback of this method are the high costs of commonly used noble metals [4-5], owing their excellent catalytic activities for hydrogen production [6]. In the search of lower cost alternatives, the catalytic properties of Ni, Mo, Fe, Rh, and alloys of these metals have been explored. Some of the most important and studied metal catalysts are binary or ternary codeposits of Ni, such as NiZn, NiCo, NiW, NiMo, NiFe and NiCr [7]. In particular, the NiMo system has shown superior electrocatalytic activity compared to bare nickel and other nickel alloys, requiring lower overpotentials for hydrogen evolution [7-9]. This improved performance of the NiMo system has been attributed to a cooperative electronic functioning mechanism of the alloy components involved [10]. NiMo materi-

als have also shown an advantageous electrochemical corrosion resistance and long term stability [7]; such characteristics have prompted investigation on the effect of factors, such as composition, nanostructure, or nanoparticle size on the performance of these materials. Consequently, it is convenient and often of interest in the catalysis field, as well as for applications in electronics and data storage, to count on approaches for fabrication of nanostructured materials at low cost, certainly rapid, and scalable for industrial production. Electrodeposition is a highly convenient procedure for such applications; multiparticulate materials are made in relatively short times, allowing quick screenings on the effect of synthesis conditions on the material properties. In particular, the electrocatalytic performance of NiMo multiparticulate systems depends on the fabrication conditions [11], which in turn may be tied up to their nanostructure (i. e. morphology and particle size) and composition [11]. The crystalline structure of NiMo materials is another parameter affecting the electrocatalytic performance of NiMo materials for hydrogen evolution [12, 13].

Electrodeposition of metallic nanoparticles is achieved either through the application of a double potential pulse or by means of

*To whom correspondence should be addressed: Email: mvidea@itesm.mx
Phone: 52 (81)83284489

a single current pulse. The former method has been extensively explored for this purpose [14, 15]; however, the application of a single current pulse has shown some advantages over the double potential technique in terms of controlling size and size distribution of Ni nanoparticles [16]. The electrodeposition of Ni nanoparticles using both techniques was recently reported [16]; lower density (nanoparticles per unit area of substrate) and faster growth of nanoparticles were determined with the double potential pulse method, whereas better control of nanoparticle size (narrower size distributions and smaller standard deviations) was observed when a single current pulse of 90 or 110 milliseconds was applied.

The purpose of this work was to explore the pulse current technique for electrodeposition of NiMo nanoparticles on glassy carbon substrates and further characterize their catalytic performance for the electrochemical production of hydrogen.

2. EXPERIMENTAL

The composition of the electrolytic bath used for NiMo alloy deposition contained the following, 0.2M NiSO₄·6H₂O (Sigma Aldrich), 0.06M Na₂MoO₄·2H₂O (Mallinckroft Chemical Works), 0.136M Na₃C₆H₅O₇·2H₂O (Baker Analyzed Reagent) and deionized water; the pH was adjusted to 9.0 adding NH₄OH. Electrodeposition experiments were performed using a three-electrode arrangement connected to an EG&G PAR potentiostat/galvanostat, model 273A. The working electrode was made from a glassy carbon (GC) rod, encapsulated in a resin and only exposing the cross sectional area (0.07 cm²). Prior to each experiment, the working electrode was polished with alumina suspensions with particle diameters of 1, 0.1 and 0.02 μm. After polishing, the electrode was rinsed with deionized water and cleaned by immersion in an ultrasonic bath for 30 seconds. A Hg/Hg₂SO₄ electrode (0.641 V vs SHE) was utilized as reference and the auxiliary electrode consisted of a platinum mesh. Electrodes were fitted into a teflon cap to hold them in position and placed in a glass cell containing 50 mL of the electrolyte solution. The pulse duration was kept constant at two seconds in all electrodeposition experiments, whereas the pulse current density was varied in the range of 7 and 430 mA/cm². The cyclic voltammetry technique was used to characterize the electrocatalytic activity of NiMo deposits; each deposit was transferred to a 0.78M H₂SO₄ solution, and a potential sweep from the open circuit potential of the system (usually -0.4 V vs Hg/Hg₂SO₄) to -0.9V, and back to the starting potential was performed. The catalytic activity of the deposit for the hydrogen evolution reaction (HER) was a direct measure of the current generated at a potential of -0.9 V vs Hg/Hg₂SO₄.

Electrodeposited NiMo materials were visualized under a FEI scanning electron microscope (Nova Nano SEM 200), and images captured at an accelerating voltage of 15 kV. Quantitative compositional analysis of deposits was conducted by means of energy dispersive X-ray spectrometry (EDXS) coupled to the scanning electron microscope.

Nanoparticle size was quantitatively measured by image analysis (Image J, NIH, Baltimore, MD); processing of original SEM files consisted of binary image reconstruction at a predetermined grayscale threshold. Approximately 300 in-focus objects were measured to obtain statistically representative determinations of mean nanoparticle diameter.

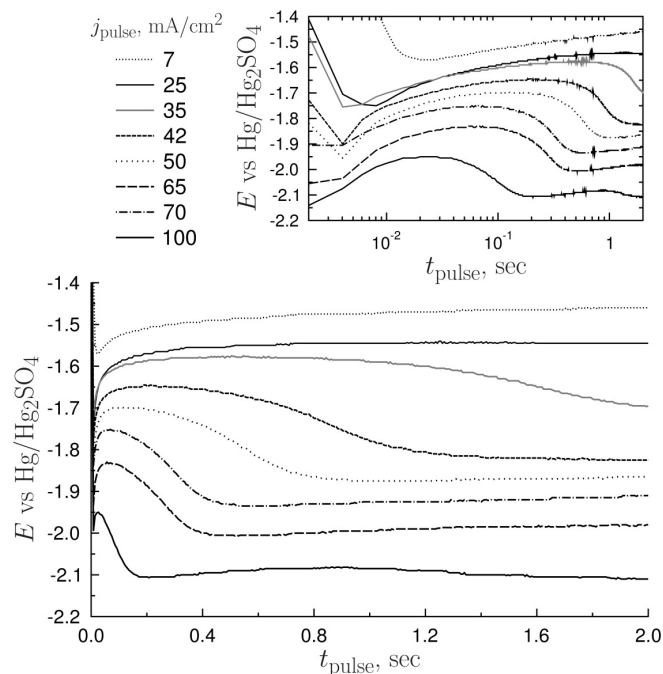


Figure 1. Potential versus time curves generated during electrodeposition of NiMo nanoparticles at different pulse current conditions. In the inset, the time-axis is in logarithmic scale.

3. RESULTS AND DISCUSSION

3.1. Polarization potential curves

Fig. 1 shows potential versus time curves generated during electrodeposition of NiMo nanoparticles on glassy carbon (GC) substrates and using variable pulse current density, j_{pulse} ; the pulse time, t_{pulse} , was kept the same (two seconds) in all cases. A fast polarization leading to a minimum and a recovery towards a steady state was observed at j_{pulse} values above 35 mA/cm². However, at a j_{pulse} equal or higher than 35 mA/cm², the potential drops again and a second minimum becomes apparent at longer times; this is remarkable in the inset of Fig. 1, where the x-axis scale is logarithmic. In the inset it can be observed that the first minimum occurs within the first milliseconds of polarization. Data acquisition limitations do not allow a clear definition of these minima at the largest current pulse densities, but there is a clear recovery in the electrode potential and a second minimum is observed; it is near to 1 second for the 42 mA/cm² pulse and shifts to shorter times as the current pulse density increases. It appears close to 0.2 sec for the 100 mA/cm² pulse.

The appearance of a second minimum suggested that two different materials were being deposited at current densities equal or higher than 35 mA/cm², which was further confirmed by means of cyclic voltammetry.

3.2. Electrocatalytic activity

The electrocatalytic performance of deposits fabricated using variable pulse current density and identical pulse duration was characterized by means of cyclic voltammetry (Fig. 2). The current density associated with the hydrogen evolution reaction, j_{HER} , was

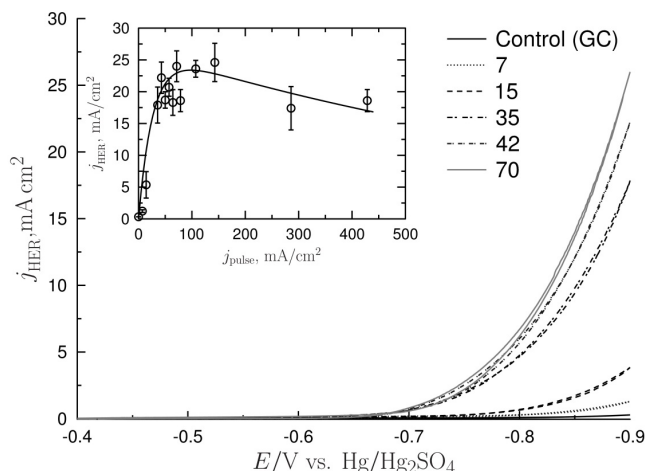


Figure 2. Cyclic voltammograms generated by deposits fabricated at j_{pulse} values of 7, 15, 35, 42 and 70 mA/cm². Inset plots the current generated -0.9V vs Hg/HgSO₄, *i. e.* j_{HER} , as function of j_{pulse} .

taken as a direct measure of the electrocatalytic activity; this value was obtained from readings at a potential of -0.9 V vs Hg/HgSO₄. Fig. 2 shows cyclic voltammograms generated by materials electrodeposited at j_{pulse} values of 7, 15, 35, 42 and 70 mA/cm² and using a $t_{\text{pulse}} = 2$ seconds, in all cases. Inset in Fig. 2 plots the current measured at -0.9 V vs Hg/HgSO₄, *i. e.* j_{HER} , against the pulse current density, j_{pulse} , applied to fabricate the deposit. The activity of deposits rapidly increased as the j_{pulse} value reached 35mA/cm², and was highest for electrodeposits obtained at current densities between 70 and 100 mA/cm², remaining practically unvaried and dropping at j_{pulse} values greater than 100mA/cm².

Tafel parameters for these experiments and j_{HER} values are shown in Table 1. The values obtained for the exchange current density are similar for all the deposits, but there is a significant difference in the values for the Tafel slope for the deposits prepared at the lower current densities which are 473 and 355 mV dec⁻¹, for 7 and 15 mA/cm², respectively. These values may be explained in terms of the total area of the deposit available for electrocatalysis since the surface area and the intrinsic catalytic activity of the deposit are entangled. At the highest current densities slightly larger values for the Tafel slope are consistent with a decrease in the currents densities, j_{HER} , obtained at a polarization of -0.9 V vs Hg/Hg₂SO₄.

3.3. Electrochemical stability

Fig. 3 shows cyclic voltammograms of a deposit fabricated at a pulse current density (j_{pulse}) and time (t_{pulse}) of 70 mA/cm² and two

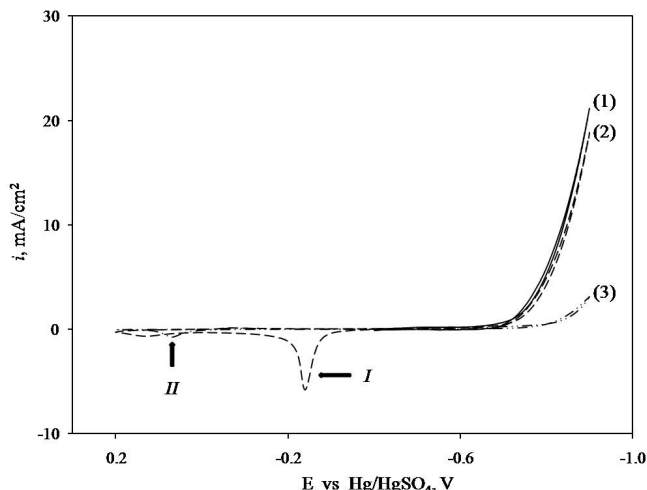


Figure 3. Cyclic voltammograms for a NiMo deposit fabricated at $j_{\text{pulse}} = 70$ mA/cm² and $t_{\text{pulse}} = 2$ seconds. Three consecutive cycles included: (1) sweeping the potential from -0.4V to -0.9V to screen the hydrogen evolution current; (2) the potential was taken to 0.2V, where anodic peaks *I* and *II* were observed; and in the third cycle, (3), peak *I* was not longer observed.

seconds, respectively; three consecutive cycles were performed. The first cycle started at an open circuit potential of -0.4V towards -0.9V vs Hg/HgSO₄; an exponential increase in current, due to hydrogen evolution started at approximately -0.7 V. In a subsequent cycle, performed immediately after, the potential was taken to -0.9V and then to 0.2V. The anodic peak observed at a potential of -0.241 V was associated to the oxidation of a material called *I*. A second peak, smaller and wider generated at 0.128 V vs Hg/HgSO₄ was related to a second material, named *II*. These observations were consistent with that suggested by the potential vs. time curves shown in Figure 1, which indicate the electro-synthesis of two different materials. A third consecutive cycle caused a dramatic drop in the current at -0.9V, and only ~20% of the current generated in the first cycle remained. Furthermore, when sweeping the potential now towards positive values, only the *II* peak was observed and slightly shifted towards more negative potentials. Conclusions drawn from these results were that material type *I*, removed during the second cycle, had higher electrocatalytic activity, but lower stability than material type *II*. In the following, material type *I* recall the most active one, which oxidizes at -0.241 V vs Hg/Hg₂SO₄, whereas material *II* refers to that oxidizing at 0.128 V vs Hg/Hg₂SO₄. Fig. 4 shows cyclic voltammograms of deposits fabricated

Table 1. Tafel parameter for the hydrogen evolution reaction on deposits prepared at different pulse current densities.

	Pulse current density, j_{pulse} , mA/cm ²								
	7	15	25	42	70	100	140	286	429
log (j_0 , A/cm ²)	-3.8	-3.9	-3.8	-3.9	-3.9	-3.9	-4.0	-4.0	-3.9
Tafel slop (mV/dec)	473	355	99.6	91.6	86.1	93.1	83.1	114	97.8
j_{HER} (mA/cm ²) at -0.9V vs. Hg/Hg ₂ SO ₄	1.2	5.4	17.8	22.2	24	23.6	24.6	17.4	18.9

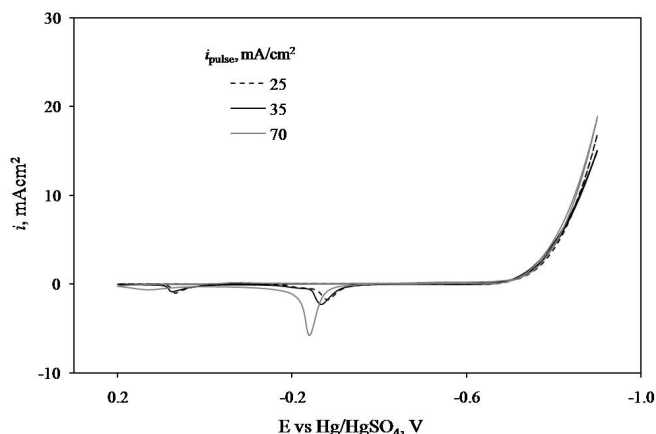


Figure 4. Cyclic voltammetry of deposits obtained at pulse current densities of 25, 35 and 70 mA/cm² show differences in areas of peaks I and II.

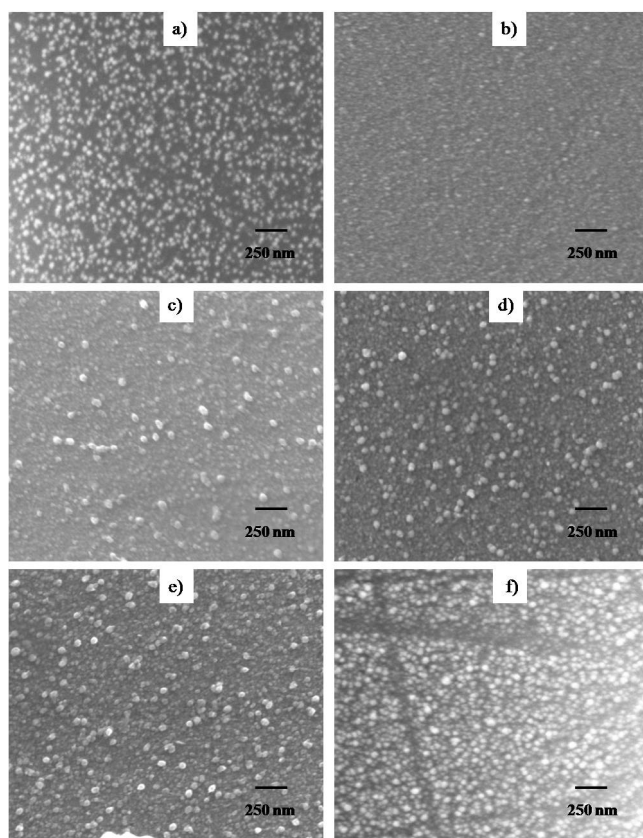


Figure 5. Scanning electron images of electrodeposits fabricated at 15, 35, 50, 70, 100 and 140 mA/cm² are respectively shown in a), b), c), d), e) and f).

at different pulse current density, where the area under the oxidation peak I was greater as the pulse current density, j_{pulse} , was also higher, suggesting that the amount of this material increased with j_{pulse} . The area under the peak II remained essentially constant upon varying j_{pulse} .

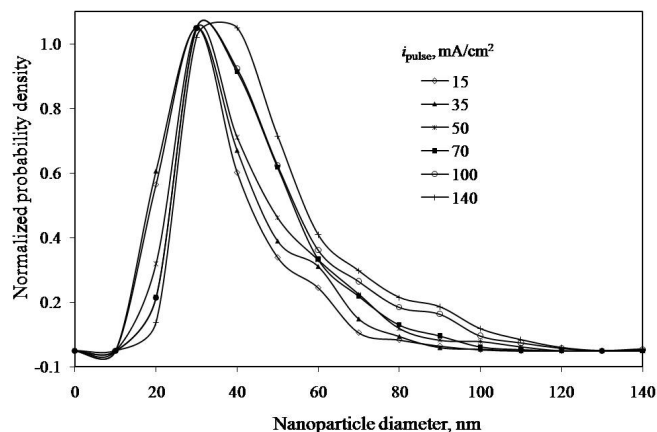


Figure 6. Size distributions of nanoparticles electrodeposited at j_{pulse} values in the range of 15 to 140 mA/cm²; t_{pulse} was equal to two seconds in all cases.

3.4. Nanoparticle dispersion and size

Fig. 5 shows scanning electron microscopy (SEM) images of electrodeposits fabricated at different pulse current density, j_{pulse} , and using a pulse time, t_{pulse} , of two seconds in all cases. The pulse current density was 15, 35, 50, 70, 100 and 140 mA/cm² respectively in Figs. 5 a), 5 b), 5 c), 5 d), 5 e) and 5 f). Nanoparticles (NPs) were observed in all cases; however, nanoparticle dispersion (*i. e.* number of objects per unit of substrate area) was lower (~150 per μm^2) in the deposits obtained at 15 and 35 mA/cm² in comparison to those fabricated at higher j_{pulse} values, suggesting that at higher pulse current density, nuclei formation is being promoted [16]. At j_{pulse} values equal or higher than 50 mA/cm², NP dispersion was approximately 300 per μm^2 and did not significantly changed upon varying the pulse current density. A mean nanoparticle diameter, D_{mean} , of 27.6, 29.7, 32.8, 34.3, 36.1 and 38.1 was respectively determined for j_{pulse} values of 15, 35, 50, 70, 100 and 140 mA/cm²; this increase in D_{mean} with j_{pulse} was consistent with an extended stabilization or growth phase observed in polarization curves upon increasing the pulse current density [16].

Fig. 6 shows the effect of pulse current density, j_{pulse} , on NP size distributions; in all cases the deposition pulse time, t_{pulse} , was equal to two seconds. Narrower distributions were seen when j_{pulse} was either 15 or 35 mA/cm² in comparison to those obtained at higher j_{pulse} values. Upon increasing j_{pulse} , distributions shifted towards larger diameters and the probability density increased in the range of 40 nm \leq NP diameter \leq 120 nm, suggesting higher counts of NP sizes within that range. This trend, which was consistent with qualitative features of SEM images, manifested itself in a gradual increase in D_{mean} with j_{pulse} , again suggesting a promoted generation of larger NP diameters by either a high j_{pulse} value or an extended stabilization (growth) stage during electrodeposition [16].

3.5. Compositional analysis

Variations in the applied current density, j_{pulse} , affected both, Ni and Mo content of electrodeposits fabricated in the range of 15 mA/cm² $\leq j_{\text{pulse}} \leq$ 140 mA/cm² (Table 2). Ni weight percent was greater that Mo content in all fabricated deposits, however no trend was found between composition and j_{pulse} . The presence of oxygen

was evident from EDXS results presented in Table 2, and suggested that oxides formation is highly likely. A mechanism of catalytic reduction of molybdate (MoO_4)²⁻ to the metallic state by a nickel-citrate complex ($\text{Ni}(\text{Ci})$), forming the species $[\text{Ni}(\text{Ci})\text{MoO}_2]$, which further reduce to NiMo, has been proposed [17-18]. This mechanism provides insights on the way oxygen could be incorporated in the electrodeposits. Ongoing X-ray photoelectron spectroscopy (XPS) analysis will provide additional information on oxides formation, and will be helpful to understand oxygen role on the catalytic activity or whether it forms part of the deposit or not.

EDXS mapping of deposits (Fig. 7) show the Ni, Mo and O detection within deposits obtained at 15 and 70 mA/cm². Figs. 7 a), 7 c) and 7 e) show the distribution of Mo, Ni and O in the deposit fabricated at 15 mA/cm², whereas Figs. 7 b), 7 d) and 7 f) were for that deposited at 70 mA/cm². These results suggested a rather uniform composition of the material throughout the sample, in other words, an approximately identical composition is expected at any point. Similar results were seen for other j_{pulse} values, however, such analysis did not provide enough information to compositionally distinguish between materials I and II above referred. Additional X-ray photoelectron spectroscopy (XPS) analysis being undergone will be helpful to detect compositional heterogeneities throughout the samples and confirm the possible presence and distribution of two different catalytic materials (I and II) mentioned above. In addition, will aid to understand the role of each material type in the catalytic performance of deposits, as well as the pulsed current conditions at which the deposition of each material type is promoted.

4. CONCLUSIONS

The electrodeposition of NiMo nanoparticles (NPs) was successfully achieved by means of current pulses and using a binary electrolyte; nanoparticle sizes ranged between 10 and 110 nm, and mean diameter values were dependent on the pulse current density, j_{pulse} , used. Nanoparticle dispersion and mean diameter, D_{mean} , were both lower when the j_{pulse} value was also low. A prolonged nanoparticle growth and promoted nuclei formation at higher j_{pulse} values was consistent with a gradual increase of D_{mean} and higher nanoparticle counts per unit area of substrate upon increasing the j_{pulse} value. Narrower NP size distributions were obtained at smaller pulse current density values, suggesting the efficacy of the pulse current technique to control NP size. The pulsing current conditions used for NP electrosynthesis affected their electrocatalytic performance for the hydrogen evolution reaction, which was determined as the current generated at a potential of -0.9 V vs Hg/HgSO₄, *i. e.*, j_{HER} . In the range of $7 \text{ mA/cm}^2 \leq j_{\text{pulse}} \leq 70 \text{ mA/cm}^2$ the electroactivity was gradually improved upon increasing the j_{pulse} value; re-

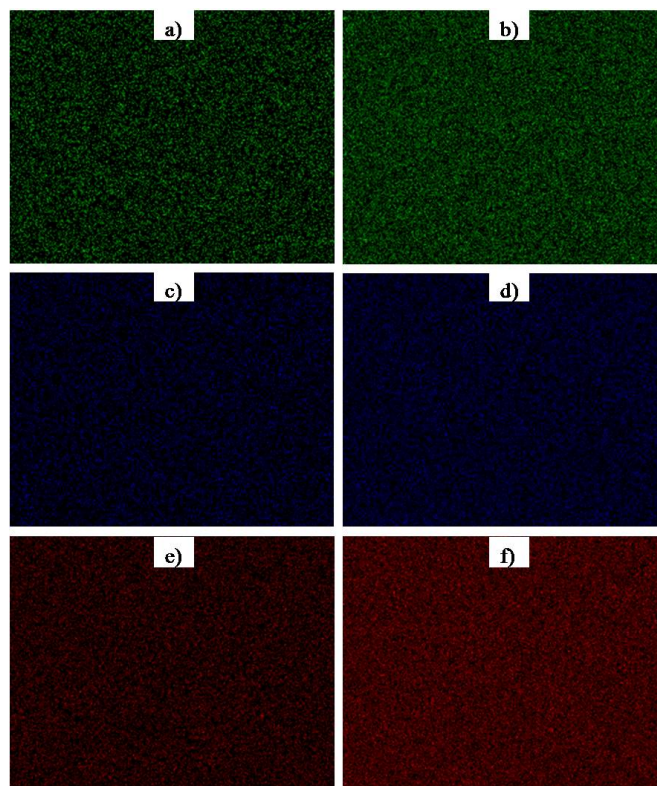


Figure 7. EDXS mapping of electrodeposits fabricated at 15 (a, c) and e)) and 70 mA/cm² (b, d) and f)). Images a) and b) present Mo distribution within the samples, whereas images c) and d) show Ni detection; O distribution is given by images e) and f).

maintaining practically unchanged upon further increasing j_{pulse} . Two catalytically distinct materials, showing different electrochemical stability, were likely present in electrodeposits, however EDXS results showed compositional uniformity at any point within the sample and further studies are needed to confirm the electrosynthesis of such distinct types of catalytic materials.

5. ACKNOWLEDGEMENTS

The authors acknowledge CONACyT for the financial support through the program Colaboración Interamericana de Materiales (No 101939). The research funding from the Tecnológico de Monterrey, Campus Monterrey, through the research grant CAT120 is also greatly acknowledged.

Table 2. Composition of NiMo nanoparticles electrodeposited at different pulsing current conditions.

Content, % weight	Pulse current density, j_{pulse} , mA/cm ²					
	15	35	50	70	100	140
Ni	53.6	54.0	42.6	72.8	46.9	66.4
Mo	10.6	12.4	16.1	4.2	6.3	6.8
O	35.8	33.6	41.3	23.0	46.8	26.8

REFERENCES

- [1] L.P. Bicelli, *Int. J. Hydrogen Energy*, 11, 555 (1986).
- [2] N. Getoff, *Int. J. Hydrogen Energy*, 15, 407 (1990).
- [3] M. Hoel, S. Kvemdokk, *Resour. Energy Econ.*, 18, 115 (1996).
- [4] F. Li, I. Ciani, P. Bertocello, P.R. Unwin, J. Zhao, C.R. Bradbury, D.J. Fermin, *J. Phys. Chem. C*, 112, 9686 (2008).
- [5] F.W. Campbell, S.R. Belding, R. Baron, L. Xiao, R.G. Compton, *J. Phys. Chem. C*, 113, 14852 (2009).
- [6] M.K. Neylon, S. Choi, H. Kwon, K.E. Curry, L.T. Thompson, *Appl. Catal. A-Gen.*, 183, 253 (1999).
- [7] I.A. Raj, K.I. Vasu, *J. Appl. Electrochem.*, 20, 32 (1990).
- [8] E. Navarro-Flores, Z. Chong, S. Omanovic, *J. Mol. Catal. A-Chem.* 226, 179 (2005).
- [9] A. Damian, S. Omanovic, *J. Power Sources* 158, 464 (2006).
- [10] S. Martinez, M. Metikos-Hukovic, L. Valek, *J. Mol. Catal. A-Chem.*, 245, 114 (2005).
- [11] M. Videa, D. Crespo, G. Casillas, G. Zavala, *J. New Mat. Electr. Sys.*, 13, 239 (2010)
- [12] L. Huang, F.Z. Yang, S.K. Xu, S.M. Zhou, T.I. Met. Finish., 79, 136 (2001).
- [13] R. Schulz, J.Y. Hout, M.L. Trudeau, L. Dignard-Bailey, Z.H. Yan, S. Jin, A. Lamarre, E. Ghali, A. Van Neste, *J. Mater. Res.*, 9, 2998 (1994).
- [14] E. Budevski, G. Staikov, W.J. Lorenz, *Electrochim. Acta*, 45, 2559 (2000).
- [15] M. Ueda, H. Dietz, A. Anders, H. Knepe, A. Meixner, W. Plieth, *Electrochim. Acta*, 48, 377 (2002).
- [16] G.T. Martinez, G. Zavala, M. Videa, *J. Mex. Chem. Soc.*, 53, 7 (2009).
- [17] E.J. Podlaha, D. Landolt, *J. Electrochem. Soc.*, 143, 885 (1996).
- [18] E.J. Podlaha, D. Landolt, *J. Electrochem. Soc.*, 144, 1672 (1997).